

**PHS PUBLIC ACCESS**

Author manuscript

ACS Infect Dis. Author manuscript; available in PMC 2017 March 11.

Published in final edited form as:

ACS Infect Dis. 2016 March 11; 2(3): 194–206. doi:10.1021/acsinfecdis.5b00102.

**Identification of small molecule inhibitors that block the *Toxoplasma gondii* rhoptry kinase ROP18****Catherine Simpson<sup>1,a</sup>, Nathaniel G. Jones<sup>2,a</sup>, Emily A. Hull-Ryde<sup>1</sup>, Dmitri Kireev<sup>1</sup>, Michael Stashko<sup>1</sup>, Keliang Tang<sup>2</sup>, Jim Janetka<sup>3</sup>, Scott A. Wildman<sup>3,b</sup>, William J. Zuercher<sup>4</sup>, Matthieu Schapira<sup>5,6</sup>, Raymond Hui<sup>5,7</sup>, William Janzen<sup>1,\*c</sup>, and L. David Sibley<sup>2,\*</sup>**<sup>1</sup>Center for Integrative Chemical Biology and Drug Discovery, UNC Eshelman School of Pharmacy, University of North Carolina, 125 Mason Farm Road, CB#7363, Chapel Hill, NC 27599-7363<sup>2</sup>Department of Molecular Microbiology, Washington University Sch. Med. St. Louis MO 63110<sup>3</sup>Department of Biochemistry and Molecular Biophysics, Washington University Sch. Med. St. Louis MO 63110<sup>4</sup>SGC-UNC, Division of Chemical Biology and Medicinal Chemistry, UNC Eshelman School of Pharmacy, 120 Mason Farm Rd, 1070H Genetic Medicine Building, University of North Carolina, NC 27599-7363<sup>5</sup>Structural Genomics Consortium, University of Toronto, MaRS South Tower, 101 College St, Toronto, ON, M5G 1L7, Canada<sup>6</sup>Department of Pharmacology and Toxicology, University of Toronto, 1 King's College Circle, Toronto, ON M5S 1A8, Canada<sup>7</sup>Toronto General Hospital Research Institute, 200 Elizabeth St., Toronto, ON M5G 2C4, Canada**Abstract**

The protozoan parasite *Toxoplasma gondii* secretes a family of serine-threonine protein kinases into its host cell in order to disrupt signaling and alter immune responses. One prominent secretory effector is the rhoptry protein 18 (ROP18), a serine-threonine kinase that phosphorylates immunity

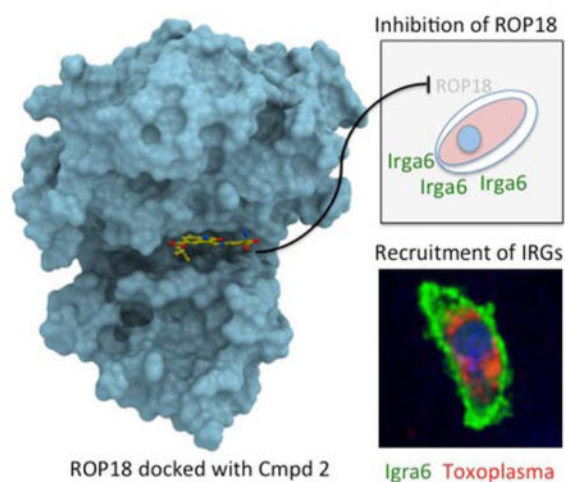
\*Corresponding authors: L. David Sibley, [sibley@wustl.edu](mailto:sibley@wustl.edu), William Janzen, [wjanzen@epizyme.com](mailto:wjanzen@epizyme.com).<sup>a</sup>Contributed equally<sup>b</sup>Current address: Carbone Cancer Center, School of Medicine and Public Health, University of Wisconsin, Madison, Wisconsin<sup>c</sup>Current Address: Epizyme, Inc., 400 Technology Square, 4th Floor, Cambridge, MA 02139**Author contributions.**

CS, EAHR, M Stasko, KT: Designed and performed the enzyme assays and HTS NGJ: Designed and performed biological experiments and analysis of human targets M Schapira, RH: Designed and performed the structural docking studies BZ, DK, JJ, SAW: Provided SAR and input on the chemical inhibitors WJ, LDS: Supervised the project and wrote the paper (with input from all authors).

Supporting information. Additional data and features of compounds **2** and **7** are found in the Supplementary Information. This information is available free of charge via the internet at <http://pubs.acs.org>.Figure S1 Mechanism of inhibition of compound **2**Figure S2 Mechanism of inhibition of compound **7**Figure S3 2-D plots for interactions of compounds **2** and **7** with ROP18.Figure S4 Overlay of interaction of compounds **2** and **7** with ROP18.Figure S5 The human kinome with results of compound **2** profiling overlaid.Table S1 Inhibition of human kinases by compound **2**.

related GTPases (IRGs) and hence blocks interferon gamma-mediated responses in rodent cells. Previous genetic studies show that ROP18 is a major virulence component of *T. gondii* strains from North and South America. Here, we implemented a high throughput screen to identify small molecule inhibitors of ROP18 *in vitro* and subsequently validated their specificity within infected cells. Although ROP18 was not susceptible to many kinase-directed inhibitors that affect mammalian kinases, the screen identified several sub micromolar inhibitors that belong to three chemical scaffolds: oxindoles, 6-azaquinazolines, and pyrazolopyridines. Treatment of interferon gamma-activated cells with one of these inhibitors enhanced immunity related GTPase recruitment to wild type parasites, recapitulating the defect of *rop18* mutant parasites, consistent with targeting ROP18 within infected cells. These compounds provide useful starting points for chemical biology experiments or as leads for therapeutic interventions designed to reduce parasite virulence.

## Graphical Abstract



The serine threonine kinase ROP18 is an important virulence factor of *Toxoplasma gondii*. ROP18 phosphorylates the immunity related GTPases such as Irga6, rendering them incapable of clearing parasites in interferon activated cells. The present work identifies inhibitors of ROP18 that block its ability to thwart IRG recruitment in interferon-activated cells.

## Keywords

interferon; phosphorylation; high throughput screening; pathogen; virulence; toxoplasmosis

## Introduction

*Toxoplasma gondii* is a protozoan parasite that infects a wide range of warm-blooded hosts, including wild, companion, and agricultural animals<sup>1</sup>. *Toxoplasma* is naturally transmitted by infection of rodents, which serve as intermediate hosts, and members of the cat family (Felidae), where sexual development in the intestinal epithelium leads to shedding of spore-like oocysts into the environment<sup>1</sup>. Humans become infected by ingestion of tissue cysts,

which are associated with chronic infections in food animals, or ingestion of food or water that is contaminated with oocysts<sup>2,3</sup>. Although healthy individuals are normally able to control the infection, chronic stages are thought to persist for life, leading to the risk of reactivation in the event the immune system wanes or becomes compromised<sup>4</sup>. Limitations of existing therapies include drug intolerance, adverse effects of treatment, and an inability to eradicate the chronic tissue cyst forms of the infection<sup>5</sup>.

*Toxoplasma gondii* has a highly unusual population structure that is dominated by three closely related clonal lineages that exist in North American and Europe where they are thought to have arisen recently as the product of a few genetic crosses in the wild, followed by recent expansion<sup>6,7</sup>. In contrast, strains of *T. gondii* from South America are genetically diverse and show greater evidence of genetic recombination<sup>8-10</sup>. Crosses between the clonal strains have been used to map the genetic basis of difference in acute virulence in laboratory mice based on differences in time to death, LD<sub>50</sub>, or lethality vs. chronicity<sup>11</sup>. Genetic mapping studies have identified a small number of polymorphic loci encoding rophtry (ROP) kinases or pseudokinases as important in controlling these differences<sup>11</sup>. ROP18 contributes to the high virulence of type I strains and the intermediate virulence of type 2 strains in comparison to avirulent type 3 strains. The basis for the avirulence in type 3 was shown to be due to under-expression of ROP18, and virulence was restored when ROP18 from type 1 or 2 was re-expressed<sup>12,13</sup>. Consistent with this, deletion of ROP18 in a type 1 background led moderate decreases in virulence of the RH strain<sup>14</sup> and a much stronger phenotype in the type 1 strain GT-1, which was used in the original cross<sup>15</sup>. ROP18 alleles in South American strains also resemble type 1 alleles<sup>16</sup>, and recent genetic studies reveal that ROP18 also plays a critical role in mouse virulence of these diverse lineages<sup>17</sup>. The other major virulence determinant in the mouse is ROP5, a polymorphic locus of tandemly repeated genes that contributes to the acute virulence of type 1 strains, yet the corresponding cluster of ROP5 alleles in type II strains decreases virulence<sup>18,19</sup>.

Rodents are a natural host for *T. gondii*, and the major virulence factors that have been identified in this system target innate and adaptive immune responses that are important in control of infection<sup>20</sup>. ROP18, ROP5, and a related kinase ROP17 are key participants in this dynamic. ROP18 and ROP17 are active kinases that phosphorylate immunity related GTPases<sup>14,21,22</sup>, which are upregulated by interferon- $\gamma$  (IFN- $\gamma$ ) and contribute to clearance of susceptible type 2 and 3 strain parasites<sup>23-25</sup>. ROP17 and ROP18 show a preference for conserved Thr residues that occupy switch region 1<sup>14,21,22</sup>, a flexible loop in the GTPase that is critical for binding nucleotides and for oligomerization. The major allele of ROP5 from type 1 strains both enhances the activity of ROP18<sup>26</sup> and also binds directly to monomeric IRGs<sup>27,28</sup>, hence providing them as substrates for phosphorylation. ROP18 has also been shown to phosphorylate ATF6 $\beta$ , a transcription factor important in the unfolded protein response<sup>29</sup>. Disruption of ATF6 $\beta$  in dendritic cells leads to impaired CD8 T cell development<sup>29</sup>, suggesting that ROP18 also disrupts adaptive immunity. Although IRGs are largely confined to rodent and not thought to participate in human resistance to toxoplasmosis<sup>30</sup>, ATF6 $\beta$  is conserved and may also be important in a wide range of hosts. Virulent alleles of ROP18 are associated with more severe ocular disease in patients from Colombia<sup>31</sup>, suggesting this factor may also contribute to severity of human infection.

Like their eukaryotic hosts, protozoan parasites contain a variety of protein kinases that comprise the major families of protein kinases with the exception of tyrosine kinases<sup>32</sup>. Protein kinases have been useful targets for development of therapeutic agents in humans, with more than two dozen drugs being approved for cancer treatment in recent years<sup>33</sup>. Given the importance of protein kinases, which in many cases control essential aspects of parasite biology, it has been suggested they may be effective targets for the development of drugs to combat infection<sup>34</sup>. Efforts have been undertaken to screen the kinome of *Plasmodium* to define essential genes<sup>35,36</sup>, and thereby prioritize essential targets. Proteomic and computational studies indicate that the *T. gondii* genome encodes ~ 160 kinases or pseudokinases, of which ~45 are thought to be contained in the rhoptry<sup>37-39</sup>. ROP kinase expansion is shared among closely related tissue cyst forming coccidians but they are not found broadly in the Apicomplexa<sup>39</sup>. Approximately half of the ROP kinases are predicted to be enzymatically active, while the other half, like ROP5 lack an intact catalytic triad and are likely not catalytically competent<sup>38</sup>. Crystal structures are available for ROP2/ROP8<sup>40</sup>, two pseudokinases that lack ATP binding, and also for ROP5<sup>41</sup>, which binds ATP in an unconventional manner, and it is unlikely to catalyze hydrolysis. A recent crystal structure of ROP18 confirmed that it shares many features in common with the ROP2 sub-family, including an N-terminal extension of the N-lobe, which in mutational studies has been shown to be important in regulating activity<sup>40</sup>. ROP kinases are highly divergent, and do not closely resemble any of the major kinase families of eukaryotes<sup>39</sup>. Although ROP18 is not essential for growth, inhibitors that block its activity would be expected to decrease pathogenesis, a strategy that has been suggested to focus on pathogens over commensals while exerting less selective pressure for resistance<sup>42</sup>.

Given the importance of ROP18 in controlling virulence in the mouse model, we were interested in identifying chemical inhibitors that could be used to probe the function of this kinase and if possible to block its activity to prevent virulence. We undertook a small molecule screen to identify specific inhibitors of ROP18. We identified multiple chemical scaffolds as low to sub micromolar inhibitors of ROP18 including oxindoles, pyridopyrimidines, pyrazolopyridines, and as well as several staurosporine-like compounds. Using a secondary assay to assess ROP18 biological function, we were able to confirm that one of these compounds target ROP18 in cells, blocking its ability to prevent IRG recruitment. These compounds may thus be useful to assess the function of ROP18 in host cells in a temporally controlled manner and without the need for genetic deletion from the parasite. The oxindole compound **2** has low host cell toxicity, and thus represents a promising lead for designing more potent inhibitors with greater selectivity, that could potentially be used to assess ROP18 inhibition *in vivo*.

## Results and Discussion

### Development of a High Throughput Screening assay for ROP18

To facilitate screening of ROP18 inhibitors, we developed a High Throughput Screening (HTS) compatible kinase assay using microfluidic capillary electrophoresis (MCE)<sup>43,44</sup>. In MCE, the phosphorylated and unphosphorylated forms of fluorescently labeled substrate peptides are separated and analyzed through a LabChip EZ Reader (Perkin Elmer). We

initially evaluated substrate peptides based on a native substrate of ROP18 from switch region 1 of Irga6 (FL-T: 5-Fam-GAAKTGVVEVT-Nle-KR-NH<sub>2</sub>)<sup>14, 21</sup>, as well as a mutant that altered the first T to E (FL-E: 5-Fam-GAAKEGVVEVT-Nle-KR-NH<sub>2</sub>). We compared these two substrates since ROP18 has been shown to phosphorylate both Thr residues, which might potentially complicate the analysis of inhibitors. We also screened a library of known MCE compatible kinase substrate peptides (kindly provided by Perkin Elmer) to determine their suitability as substrates for ROP18. One such peptide (FL-8: 5-FAM-IPTSPITTTYFFFKKK-COOH) that is a known substrate of ERK1,2 / p38 also proved to be a good substrate for ROP18, presumably because of the repeated TTT sequence, a motif that is preferred by ROP18<sup>21</sup>.

Fam-conjugated peptide substrates (1 μM) were incubated with recombinant ROP18 recombinant protein and varying concentrations of ATP for 1 h and samples were resolved on a LabChip MCE platform. Analysis using Michaelis-Menton kinetics revealed an ATP  $K_m$  of approximately 15 μM for both FL-T and FL-E, and 3 μM for FL-8 (Figure 1 a–c). Reactions containing 1 μM of FL-T, 60 μM ATP, and varying concentrations of ROP18 were incubated to determine the extent of conversion of the peptide to the phosphorylated form over 3 h at room temperature (Figure 1d). Finalized reactions containing 1 μM FL-T, 60 μM ATP, 75 nM ROP18, and 1% DMSO incubated for 3 h using assay conditions defined in Table 1. This method resulted in approximately 30% conversion of substrate to product, which lies within the linear range of the reaction and is ideal for detecting inhibitors by MCE<sup>45–47</sup>, while also allowing us to conserve enzyme over multiple runs.

The assay was then transitioned into a HTS format. Additions were performed using a Multidrop Combi for addition of enzyme, substrate, and positive and negative controls. Inhibitors to the 384 well plates were added with the NanoScreen liquid and plate handler. For HTS screening, each plate included negative controls (no ROP18, for 100% inactive, containing 1% DMSO) in rows 1 and 2, while positive controls (containing ROP18 and 1% DMSO but no inhibitor) occupied rows 23 and 24. Repeated runs using this configuration to monitor ROP18 phosphorylation yielded results consistent with HTS standards (i.e. Coefficient of Variation (CV) <10% and  $Z'$  > 0.5<sup>48</sup>). We then used a test library of inhibitors to validate the reproducibility for the FL-T screen. The 906 compound Published Kinase Inhibitor Set (PKIS) (GlaxoSmithKline (GSK)) library was run in duplicate on a single day (4 plates total). The assay demonstrated excellent results with  $Z'$  values > 0.9 for all plates and a high degree of correlation between duplicate runs (Figure 2).

Using this validated HTS assay, we undertook a discovery effort for ROP18 inhibitors by screening both the GSK PKIS and a previously assembled set of ~ 5,000 small molecules held in the University of North Carolina (UNC) Center for Integrative Chemical Biology and Drug Discovery (CICBDD) compound collection<sup>49, 50</sup>.

### Analysis of hits from the HTS

Prior to undertaking the HTS, we tested a set of 32 known kinase inhibitors selected for broad kinome coverage by the CICBDD in dose response format. The known kinase inhibitor plate generated 3 hits with IC<sub>50</sub> < 1.5 μM (Table 2, compounds **14–16**). These compounds were all broad-spectrum kinase inhibitors, including staurosporine, and two

related analogs lesaurtinib and K252a (Table 2). Although these compounds were potent inhibitors of ROP18, they are known to have broadly promiscuous activity against human kinases and hence they were not pursued further here.

The primary HTS screen tested 5,665 compounds using the MCE assay platform as described in the Methods. The compounds screened consisted of focused libraries selected for either known activity against kinases or similarity to known inhibitors of kinases. These included the 4,727 member kinase-directed library prepared and provided by the CICBDD<sup>49,50</sup>(22, 40) (23, 41), and the first and second generation GSK PKIS libraries<sup>51</sup> that contain 906 compounds in total.

Compounds exhibiting >50% inhibition of ROP18 kinase activity in the primary screen were designated 'hits' (marked red in Figure 2 and above the bar in Figure 3). These initial hits were then plated in 10-point dose response curves and tested in the same assay conditions as the primary screen against FL-T, FL-E, and FL-8 for hit confirmation, substrate specificity, and IC<sub>50</sub> values. In total there were 15 hits; 2 from the kinase-directed library and 13 from the GSK PKIS. Out of these 15 hit compounds, 13 were confirmed to be active in dose response curves, including 1 from the kinase-directed library, and 12 from the GSK PKIS. As a reference, the historical hit rate for the kinase-directed library against 20 kinase targets tested in the UNC CICBDD is 2.2%. The hit rate for this non-mammalian kinase was 0.04% for the kinase-directed library and 1.43% for the GSK PKIS. This low active rate for the kinase-directed set presumably results from structural differences between the protozoan kinase and the mammalian kinases that were used in the derivation of this cassette<sup>38–40, 52</sup>. The screen also generated 32 activators, defined as compounds where the enzymatic activity of ROP18 increased by more than 50% above the baseline control (Figure 3). Although we have not explored these activators further here, they could also be useful biological probes in future studies to interrogate the functions of ROP18 by enhancing its activity.

Interestingly, all of the inhibitors had similar potencies on different substrates that varied by 2–3 fold at most for peptides FL-T or FL-E (Table 2). This result indicates that the sensitivity of ROP18 to inhibition of phosphorylation of the two separate Thr residues in this substrate is similar, and that the potential of doubly phosphorylated substrates does not confound the analysis of potential inhibitors. The slightly higher IC<sub>50</sub> values for FL-8 may reflect the lower ATP  $K_m$  (3  $\mu$ M) for the generic substrate. The two most potent compounds from the PKIS and the kinase-focused library, compound **2** and compound **7**, showed IC<sub>50</sub> values of 0.17 and 0.30  $\mu$ M respectively. Both compounds **2** and **7** were ATP competitive using FL-T with  $K_i$  values of 130 nM and 270 nM respectively (Figure S1, S2). Together the active compounds group primarily into three chemical scaffolds, oxindoles (compounds **1–4**), 6-azaquinazolines (compounds **5–7**) and pyrazolopyridines (compounds **8–10**) (Table 2).

### Structure activity relationships (SAR)

Although the number of analogs in each of the chemical series was small, we are still able to glean some information about the relative potencies of related compounds. The oxindoles **1–4** were originally generated in a drug discovery program as ATP-competitive inhibitors of human cyclin dependent kinase 2 (CDK2)<sup>53</sup>. These compounds were included in the first generation PKIS set<sup>54</sup>. The 6-azaquinazolines **5–7**, and pyrazolopyridines **8–10** were

identified as active in a phenotypic screen for antimalarial compounds<sup>55</sup>. Both chemical series have structural features typical of ATP-competitive kinase ligands, including hydrogen bond donor and acceptor moieties that interact with the kinase hinge region. These compounds were included in the second generation PKIS. The observed activity of the three pyrazolopyridines **8–10** establishes a nascent structure-activity relationship. Compounds **9** and **10** only differ in the R1 substituent and **10** is approximately one order of magnitude more potent in all three assays, pointing to the contribution of the 2,6-difluorophenyl group at this position. Compounds **8** and **10**, which have the same R1 but different R2 substituents, are within twofold activity with FL-T and FL-E and slightly more with FL-8. The higher potency observed with R1 = 2,6-difluorophenyl relative to cyclohexyl may be explained by its ability to establish a favorable interaction with an edge or face of the aromatic ring.

### Molecular docking of candidate inhibitors

For molecular docking studies, we choose one member of each of the three major scaffolds that were identified in the screen (compounds **2**, **7**, and **10** respectively). All three chemical scaffolds that are expected to bind in the ATP-binding pocket of the kinase. To provide additional insight into their mode of binding, we used the previously described X-Ray crystal structure of ROP18<sup>52</sup> and performed molecular docking with compounds **2**, **7**, and **10**. We were not able to identify a consistent binding pose for **10**, but a reliable docking models were produced for compounds **2** and **7**. In the model, compound **2** occupies the ATP binding pocket of ROP18, and the oxindole scaffold makes a canonical double hydrogen bond with backbone atoms of M357 and A359, at the hinge region that links the N- and C-terminal lobes of the kinase (Figure 4a). Hydrogen bonds are also engaged with surrounding side-chains, between the ester carbonyl oxygen and K281, and between the sulfonamide group and two C-lobe residues (D362, K365). Most of the other analogs of this scaffold, which share the sulfonamide group but have slight differences in the substituents at C 4,5 of the oxindole core, were also potent inhibitors of ROP18 *in vitro* (Table 2). Loss of the ester carbonyl interaction with K281 may explain the lower potency of compound **1**, while substitution of *tert*-butyl alcohol group in compound **3** may preserve this interaction and hence potency.

Compound **7**, and related analogs **5** and **6** all share a 6-azaquinazoline. Molecular docking of compound **7** revealed that the pyridone moiety of compound **7** forms a double hydrogen-bond with the backbone of A359 and M357 at the hinge of ROP18 (Figure 4b), effectively mirroring interactions observed with the oxindole of compound **2**. Additionally, K365 also forms a hydrogen bond with one of the oxygen atoms in the sulfonamide in the R1 group of compound **7**, while this interaction is lost in related analogs such as compound **6**, which has a 3,5-chlorophenyl group in R1, or in compound **5**, which has a sulfone SO<sub>2</sub> group oriented in a different trajectory than that of the sulfonamide **7** (Figure S3). The R1 group interacts at the opening of the cleft in ROP18 and although differences here may influence the potency among analogs (Table 2), this region is generally less important than the hinge in affecting inhibition potency.

Out computer docking models suggest that additional substitutions on the oxindole ring, or modification of the sulfonamide to exploit interactions at the other end of the pocket, may

lead to compounds with improved physicochemical properties. For example, decorating the phenol ring of **2** or **7** may capture additional interactions with the linker region of ROP18, for example the backbone carbonyl of E360 (Figure S4 a). Alternatively, hybrid scaffold might be designed that could capture the interactions observed in each individual compound. Finally, it might be possible to exploit a side cavity that is juxtaposed to the inhibitor-binding pocket in order to increase potency and selectivity (Figure S4 b).

### Biological effects of candidate inhibitors

Compounds **2**, **7**, and **10** were profiled for toxicity against RAW 264.7 macrophages using an MTS-based assay to determine growth over 48 h (Figure 5a). The dose-response relationship was generated for all compounds to allow EC<sub>50</sub> values to be calculated. Compounds **2** and **7** were relatively well tolerated with EC<sub>50</sub> values of 7.4 μM and 14.2 μM, respectively, while compound **10** was less well tolerated and caused growth inhibition with an EC<sub>50</sub> value of 1.3 μM (Figure 5a). In order to assess the acute effects of exposure to compounds, a cytotoxicity assay was conducted based on LDH release during a 4 h incubation period. Cytolytic effects were not observed upon treatment with any compound up to 10 μM (Figure 5b). At the highest concentration of 20 μM compound **7** caused a 12% increase in LDH release, suggesting at this concentration it was mildly cytotoxic. However, it was noted that compound **10** induced rapid morphological damage to the host cells in as little as 30 min with rounding up and vesiculation of the cells (Figure 5c). These findings suggest that this compound was acutely toxic albeit not directly cytolytic. Compound **10** was previously identified as active against *P. falciparum* in growth inhibition assays when used at 2 μM compound concentration<sup>55</sup>. At this dose, it showed 99% inhibition of 3D7 strain and 75% inhibition of Dd2 strain (a multidrug resistant strain) over 48 h. In the counter screen against HepG2 hepatocarcinoma cells, the compound resulted in 78% growth inhibition over 48 h when applied at 10 μM. Similarly, we observed that this compound inhibited the growth of mouse RAW 246.7 cells with an EC<sub>50</sub> value of 1.3 μM, indicating that it has considerable toxicity. We were also unable to dock this compound to the structure of ROP18 or to establish if its mode of action is competitive with ATP. Although we have not tested this directly, it is possible that compound **10** represents a promiscuous inhibitor, a class of compounds that after works by forming aggregates or colloids that indirectly inhibit enzyme reactions<sup>56</sup>. Regardless, due to the above complications, we did not pursue this scaffold further.

Based on the findings that compounds **2** and **7** are only mildly inhibitory of cell growth but not overtly toxic, we decided to test them in a bioassay to determine if they specifically inhibit ROP18 in host cells infected with *T. gondii*. The effects of ROP18 activity can be measured by observing the reduction in IRG loading to the PVM in a recruitment assay, as described previously<sup>14</sup>. Mutants that lack ROP18 are highly susceptible to IRG recruitment, while expression of high level of the enzyme block recruitment<sup>14</sup>, presumably due to phosphorylation of these targets and disruption of their loading into the vacuole. The ability of ROP18 inhibitor compounds **2** and **7** to phenocopy genetic ablation of ROP18 was therefore assessed based on recruitment of IRGs in IFNγ-activated macrophages.



In order to determine if compounds **2** and **7** could inhibit ROP18 *in vivo*, the recruitment of Irga6 was visualized using immuno-fluorescence microscopy (Figure 6 a) and evaluated by visual assessment of positive vs. negative vacuoles (Figure 6 a–c) or by quantitative measurement of the intensity of staining (Figure 6 d,e). Compounds were applied to parasites that were allowed to invade IFN- $\gamma$ -activated RAW macrophages for 30 min prior to washing, fixing and immunofluorescence staining. As expected, wild type DMSO-treated parasites resisted the recruitment of Irga6 to the PVM while the ROP18-deficient parasites were often observed with a coat of Irga6 surrounding the PVM (Figure 6 a). Vacuoles that judged to be uniformly positive for Irga6 had a mean fluorescent intensity of ~100 units, while those that showed partial labeling had reduced mean fluorescent intensity values of ~50 units. We considered both categories as positive for recruitment of Irga6 to the PVM (Figure 6 b,c). In addition, we monitored the distribution of signal on randomly selected vacuoles, revealing that there is a wide distribution of staining intensities (Figure 6 d,e). These two methods were evaluated statistically, as described below. We initially tested compounds at concentrations of 1, 5 and 10  $\mu$ M; and only observed increased recruitment at the higher dose; hence it was used for quantitative experiments in IRG loading.

Treatment with 10  $\mu$ M compound **7** led to partial recruitment of Irga6 on a minority of vacuoles (Figure 6 a); however, this did not result in a significant increase in the proportion of Irga6 positive based on visual scoring (Figure 6 b). Treatment of *rop18* parasites with compound **7** also caused a reduction in the proportion of parasites being labeled with Irga6 (Figure 6 b), suggesting that the compound may be toxic and disrupt IRG trafficking. To remove any potential observer bias, this phenotype was assessed by quantitative immunofluorescence microscopy where Irga6 recruitment was measured over a region of interest encompassing the entire parasite/PVM in a large sample of parasites (Figure 6 d). By this quantitative assessment, no significant increase in the amount of Irga6 recruitment over the entire PVM was observed after the addition of compound **7** to wild type parasites compared to vehicle treated control samples (Figure 6 d). When compound **7** was applied to *rop18* parasites, the amount of Irga6 recruitment was significantly lower than in the vehicle treated control parasites, as described above. Due to the apparent toxicity and lack of *in vivo* specificity of compound **7**, our focus shifted towards compound **2**.

The effect of addition of 10  $\mu$ M compound **2** to wild type parasites resulted in Irga6 recruitment to PVM in IFN- $\gamma$ -activated RAW264.7 cells (Figure 6 a). Irga6 recruitment resulted in more complete staining of parasite-containing vacuoles following treatment with compound **2** when compared to parasites treated with compound **7** (Figure 6 a). Whether scored visually or monitored by quantitative immunofluorescence microscopy, this difference was highly significant (Figure 6 c,e). This increase in labeling phenocopied the *rop18* DMSO control sample (Figure 6 a,c,e), suggesting ROP18 was being inhibited *in vivo* in the wild type sample rendering the vacuole susceptible to IRG loading. Importantly the addition of compound **2** to *rop18* parasites did not lead to a significant increase or decrease in the amount of Irga6 recruitment (Figure 6 a,c,e), suggesting that compound **2** acts specifically on ROP18. Although not tested here, it is also possible that compound **2** targets ROP17, a distantly related kinase that also phosphorylates IRGs and contributes to

parasite virulence<sup>21</sup>, as dual inhibition of both kinases might appear phenotypically similar to inhibition of ROP18 alone.

Compound **2** was previously profiled as part of the GSK PKIS against mammalian PKs and has been extensively profiled *in vitro* against 220 of the 518 human protein kinases. Compound **2** exhibited > 90% inhibition at 1  $\mu$ M of human protein kinases TBK1, IKK-epsilon, MELK and CDK3/cyclinE (Table S1). It also inhibits a number of mammalian kinases at > 50% when used at 0.1  $\mu$ M, including CDK2, PDGFR $\alpha$ , and PDGFR $\beta$  (Figure S5). It is noteworthy that the predicted interactions between compound **2** and ROP18 described above are all conserved in crystallized complexes of human CDK2 and a family of oxindoles, including compound **2**<sup>53</sup>. Although compound **2** lacks specificity for TgROP18, it provides a useful chemical starting point that could allow the development of more specific inhibitors useful as research compounds. Furthermore, sequence alignment (not shown) indicates the key residues on CDK2 that interact with oxindole-based inhibitors are conserved in at least one other *Toxoplasma* protein kinase, namely TGME49\_218220, which is a predicted CDK and an orthologue of *Plasmodium falciparum* MRK. The latter has been reported to be sensitive to oxindole-containing inhibitors<sup>57</sup>, although compound **2** has not been specifically tested in this regard. Hence, although compound **2** was capable of inhibiting ROP18 within cells, and abrogating its effects on the host IRG pathway, it may also have other targets in the parasite. Hence, it would be interesting in future experiments to test the effect of compound **2** on growth of the parasite *in vitro*, although any such effect is unlikely to act on ROP18, as this kinase is not essential for growth. It may also be instructive to examine the ability of treated parasites to cause infection *in vivo* (i.e. in mice) where disruption of ROP18 activity is expected to play an important role.

In comparison, compound **7** demonstrated no clear effect on blocking ROP18 activity *in vivo* and may possess other deleterious effects on the host cell due to the reduction of Irga6 recruitment to ROP18 deficient parasites. However, compound **7** was previously reported to inhibit growth of malarial parasites in red blood cells (asexual growth) and is also much less toxic to mammalian cells. In a prior screen, it demonstrated > 95% inhibition of *P. falciparum* growth at 2  $\mu$ M and only 13% inhibition of Hep2G cells at 10  $\mu$ M<sup>55</sup>. Thus, while not being an immediately useful tool for chemical biology studies of ROP18, compound **7** might be of worth in further studies to determine if it possesses growth inhibitory effects on *T. gondii* or other apicomplexan parasites.

## Conclusions

We have developed a HTS assay to detect inhibitors of ROP18, an important virulence determinant of *T. gondii*. Although many compounds that inhibit mammalian kinases were not effective against ROP18, we successfully identified several low micromolar inhibitors of ROP18 enzyme activity *in vitro*. One of these compounds was also able to inhibit ROP18 in infected cells, pheno-copying the defect in *rop18* parasites. Compound **2** may be useful as a lead for developing more specific inhibitors to further probe the function of *ROP18 in vitro* and *in vivo* using chemical genetic approaches. One advantage of such an approach is that it allows temporal control of inhibition and does not suffer from the potential for compensatory changes that can confound conventional genetic approaches. Although the

primary role of ROP18 is in targeting IRGs, a potent immune defense in rodent, this system is largely lacking in humans<sup>30</sup>. However, ROP8 has also been shown to phosphorylate ATF6 $\beta$  and this effect is thought to compromise dendritic cells presentation to CD8<sup>+</sup> T cells<sup>29</sup>, suggesting it may also have important roles in other hosts. Thus identification of more potent and specific inhibitors of ROP18 may allow chemical genetic dissection of its roles in a variety of host and cell types.

## Methods

### Biochemical materials

Fluorescein conjugated 5-Fam-GAAKTGVVEVT-Nle-KR-NH<sub>2</sub> (FL-T) and 5-Fam-GAAKEGVVEVT-Nle-KR-NH<sub>2</sub> (FL-E) peptides were synthesized by the UNC High-Throughput Peptide Synthesis and Array (HTPSA) Core Facility and reconstituted in 100% dimethylsulfoxide (DMSO) to 1.5 mM. The fluorescently labeled 5-FAM-IPTSPITTTYFFFK-KK-COOH (FL-8) peptide was purchased from Caliper Life Sciences. ProfilerPro separation buffer and coating-reagent 8 were purchased from PerkinElmer.

### GSK PKIS library

The first- and second-generation Published Kinase Inhibitor Sets (GSK PKIS and PKIS2) Libraries<sup>51</sup> were provided by GlaxoSmithKline (GSK) and used as an assay validation library. The 906 compounds were supplied as 10  $\mu$ L samples (10 mM in DMSO) in 384-well polypropylene microplates (Grenier). On the day of screening, plates were thawed and diluted (1:10) to 1 mM (10x the final assay concentration) with assay buffer (Table 1) in a 384-well plate. A Multidrop Combi Reagent Dispenser (ThermoScientific) was used to add 9  $\mu$ L of 10% DMSO to columns 1, 2, 23, and 24 that did not contain compound and served as control columns. A MultiMek NSX-1536 assay workstation system fitted with a 384-well head (Nanoscreen) was used to transfer 1  $\mu$ L of each sample into 384-well ShallowWell Nunc assay plates (ThermoScientific).

### Kinase-directed library

The 4,727 compound kinase-directed library was prepared and provided by the UNC Center for Integrative Chemical Biology and Drug Discovery (CICBDD)<sup>49, 50</sup> (22, 40) (23, 41) (23, 41). This compound set was selected from >100,000 compounds reviewed from Life Chemicals, ChemDiv, Asinex and Enamine kinase-focused libraries based on their similarity to known kinase inhibitors as well as to compounds having a hinge-binding motif (e.g. heterocycles with a high likelihood to bind the kinase hinge motif conserved in nearly every kinase-small molecule X-ray structure) and structure/ligand-based virtual screening. Plates were prepared as described for the PKIS library on the day of screening.

### Known kinase inhibitor plate

The known kinase inhibitor plate is a single 384 well plate provided by the CICBDD and composed of 32 compounds known to inhibit kinases including chelerythrine chloride, genistein, wortmannin, tozasertib, H-89, U0126, lapatinib di-*p*-toluenesulfonate, SB 203580, SP600125, SB202190, dovitinib, tyrophostin AG490, gefitinib, lestaurtinib, dasatinib, sunitinib, malate, imatinib, masitinib, sorafenib, tofacitinib, saracatinib, K252a, PD 184352,

staurosporine, erlotinib, enzastaurin, axitinib, canertinib, GDC-094, LY294002 and quercetin. The plate was prepared using a Tecan Genesis 200 (Research Triangle Park, NC) and arrayed in 10 point, 3-fold serial dilution dose curves ranging in concentration from 10 mM to 0.0005 mM. On the day of use, plates were prepared as described the PKIS library (see above). The final top concentration in the assay was 100  $\mu$ M.

### Development of the HTS

A Multidrop Combi Reagent Dispenser (ThermoScientific) was used for the addition of all reagents to assay plates. First, 10  $\mu$ L of assay buffer was added to each well in columns 1 and 2 and served as negative control reactions. Four and one-half microliters of 2.2x enzyme solution was added to columns 3–24 of the plate. Plates were incubated at room temperature for 10 min then 4.5  $\mu$ L of 2.2x substrate solution was added to each well of the entire plate. Assay plates were incubated in the dark for 3 h at room temperature. Twenty  $\mu$ L of 70 mM EDTA (in assay buffer) was then added to columns the plates to stop the reactions. Fluorescently conjugated (FL-T) and product, phosphorylated (FL-T) were analyzed in ProfilerPro separation buffer containing 0.5% CR-8 and detected using the LabChip EZ Reader II microfluidic capillary electrophoresis assay (MCE) platform from PerkinElmer.

Because the compound libraries are dissolved in 100% DMSO, reactions containing 1  $\mu$ M FL-T, 15  $\mu$ M ATP, 75 nM ROP18 and varying concentrations of DMSO were monitored using the LabChip MCE platform to determine DMSO tolerance. There was decreased activity in reactions containing 2% DMSO, but no effect at 1% or below (data not shown). Thus, compounds were prepared as 10 mM stocks in 100% DMSO and then diluted to a final concentration of 100  $\mu$ M (1:100) in 10% DMSO resulting in a final concentration of 1%, which is well within the DMSO tolerability of the reaction.

For dose response curves, compounds were plated as 3-fold serial dilutions starting with a high concentration of 10 mM or 30 mM. The lowest concentration tested in the 10-point dose response was either 0.0005 or 0.0002 mM respectively. Dose response compound plates were prepared using a Tecan Evo robotic platform. Dose response plates were heat-sealed and stored at  $-20^{\circ}\text{C}$  until day of use. On the day of use, plates were prepared as described for the PKIS library (see above). The final highest assay concentration was either 10  $\mu$ M or 30  $\mu$ M.

### Data analysis

Screening data was analyzed using Screenable software (Screenable Solutions) to calculate the mean of the positive and negative controls, the percent inhibition (with respect to on-plate controls) for each reaction and the common assay performance measure,  $Z'$ , for each plate.  $Z' = \frac{3\sigma_{max} + 3\sigma_{min}}{|\mu_{max} - \mu_{min}|}$ . Where max is the negative control (no compound; no inhibition) and min is the positive control (70 mM EDTA; 100% inhibition). A  $Z' > 0.5$  was considered acceptable for the plate to be included in the overall data analysis. The LabChip software calculated percent conversion for each reaction.

Hits were defined as compounds that inhibited ROP18 at 50%. The 50% threshold was determined as greater than 3 standard deviations from the mean percent inhibition for the

entire screen. Dose response curves were calculated using Screenable Software by converting the % conversion to % inhibition with respect to on-plate controls and using a 3 or 4-parameter curve fit.

### Culture of parasite and host cell lines

RAW264.7 macrophages (ATCC TIB-17) were maintained in DMEM (Gibco) containing 10% defined FBS (Gibco) at 37°C, 5% CO<sub>2</sub> and passaged by dilution upon reaching confluency. *T. gondii* RH strain parasites were maintained by passage in HFFs, cultured in DMEM 3% FBS, as previously described<sup>26</sup>. The genotypes of parasites used in recruitment assays were RH *ku80 hxgprt uprt::CBR* (herein described as wild type) and RH *ku80 rop18::HXGPRT uprt::CBR* (herein described as *rop18 mutant*), as described previously<sup>58</sup>. All cultures were determined to be mycoplasma negative using the e-Myco plus kit (Intron Biotechnology).

### Cell growth assays

Compound toxicity against host cells was determined by CellTiter 96 AQueous One MTS Assay (Promega, Madison, WI). RAW cells were harvested by gently scraping in PBS, resuspended in DMEM at a concentration of 1×10<sup>5</sup> cells/ml, and seeded into 96-well tissue culture plates (Corning) at 10<sup>4</sup> per well. Cells were allowed to adhere to the plate overnight. Compounds were added to a concentration of 10 μM and serially diluted in steps of 1:3, keeping a constant volume of 100 μl/well. Vehicle addition (0.1% DMSO) and media only controls were included in each plate. Cells were incubated for 48 h at 37°C, 5% CO<sub>2</sub> after which 20 μl of MTS reagent was added to wells and plates were incubated for a further 4 h at 37°C, 5% CO<sub>2</sub>. The absorbance of the reaction product was read at 490 nm in an EL-800 Plate Reader (Biotek). Three technical replicates were performed for each sample and the assay was performed three separate times.

### Cell lysis assays

Compounds were assessed for acute cytolytic effects by performing a CytoTox 96 Non-Radioactive Cytotoxicity Assay (Promega). RAW cells were seeded into 96-well tissue culture plates at a density of 10<sup>4</sup> per well. Compounds were added and serially diluted as previously described. After 4 h incubation at 37°C, 5% CO<sub>2</sub>, 50 μL of supernatant was collected from the each well and transferred to a new 96-well plate. Wells containing untreated cells were lysed by freezing at -80°C and then thawed at 37°C, to provide a 100% lysis control. LDH assay reagent (50 μL) was added to the supernatants and incubated at room temperature, protected from light, for 30 min. The reaction was halted by the addition of stop solution and read at 490 nm in an EL-800 Plate Reader (Biotek).

### IRG recruitment assays

Recruitment of Irga6 to the parasitophorous vacuoles (PV) was used as a biological readout of ROP18 function. RAW macrophages were harvested and seeded onto coverslips in 24-well tissue culture plates (Corning Inc) at a density of 10<sup>5</sup> cells per well and allowed to adhere overnight. Monolayers were activated with 100 U/ml recombinant mouse IFN $\gamma$  (R&D Systems) and 1 ng/ml LPS (Sigma) for 24 h. Freshly harvested *T. gondii* tachyzoites

were diluted to  $10^5$  cells / ml, treated with compounds **2** and **7** at a concentration of 10  $\mu$ M for 30 min at 37°C and then applied to RAW cell monolayers. Parasites were allowed to invade for 30 min at 37°C after which the coverslips were washed 3 times with PBS, fixed with 4% formaldehyde PBS, and permeabilized with 0.05% Triton X-100 in PBS. Coverslips were blocked in 10% goat serum (Life Technologies) PBS and then stained with the mouse monoclonal antibody 10D7, which recognized GTP-bound Irga6<sup>59</sup>, at a 1:500 dilution and the rabbit polyclonal anti-TgAldolase<sup>60</sup> at 1:1,000. Alexa-fluor conjugated secondary antibodies were applied at 1:1,000 and counterstained with 0.1  $\mu$ g/ml Hoechst 33258. Coverslips were mounted in Prolong Gold Antifade reagent (Life Technologies). These experiments consisted of 3 biological replicates, with 3 technical replicates in each, between 200 and 400 parasites were imaged from these replicates per treatment group.

### Microscopic imaging and quantification of Irga6 loading

Images were acquired using a Zeiss Axioskop 2MOT Plus epifluorescence microscope equipped with a 63x oil immersion objective using Axiovision software. Vacuoles were scored as “positive” vs. “negative” based on visual assessment. In addition, quantitative measurement of digital images was conducted using Volocity software (PerkinElmer). Parasites were manually identified by drawing a region of interest around the perimeter and the mean fluorescent intensity was calculated for each parasite. The average intensity for each parasite was adjusted by subtraction of three representative background regions taken from an uninfected host cell and from two infected host cells. Samples were compared to the wild type control using a nonparametric Kruskal-Wallis test with Dunn’s correction for multiple comparisons in Prism (GraphPad).

### ROP18 cloning and protein purification

The ROP18 gene was cloned and expressed as described previously<sup>14, 26</sup>. In brief, an expression construct starting from the sequence ERAQ (Glu83 based on the second ATG of GenBank CAJ27113) and continuing through the C-terminus was cloned into pGEX-6p-1 vector between BamH1 and SalI sites with the addition of a 6xHIS tag before the stop codon. The plasmid was then transformed into *E. coli* BL21(DE3)V2RpAcYc-LIC+LamP-phosphatase cells<sup>40</sup>. A single colony was inoculated into 5 ml of TB with ampicillin (100  $\mu$ g/ml) + chloramphenicol (34  $\mu$ g/ml), and cultured overnight at 37°C. The culture was into 250 ml of fresh TB with ampicillin (100  $\mu$ g /ml) + chloramphenicol (34  $\mu$ g /ml) and grown for 6 h at 37°C. This culture was then supplemented with 1 mM IPTG and induced at 12°C overnight. The cell pellet was lysed in CelLyticB 2x (Sigma-Aldrich) supplemented with benzonase (SIGMA) and protease inhibitor cocktail (Sigma). The protein was purified with glutathione Sepharose 4B (GE-Healthcare), and dialyzed in 250 mM NaCl, 10 mM MgCl<sub>2</sub>, 20 mM Tris-HCl pH 8.0. Glycerol was added to 20% and the protein was stored at -80°C. Protein concentrations were measured by SDS PAGE separation and staining with SYPRO-Ruby (Invitrogen) in comparison to a BSA standard.

### Molecular docking

Superimposition of the ROP18-ATP complex structure (PDB code 4JRN) with a structure of CDK2 bound to an analog of compound **2** (PDB code 4FKT) indicated that the

conformation of ROP18 Lys365 was incompatible with the position of the analog. Therefore, compound **2** was docked to an *in silico* mutant of ROP18 that altered Lys365 to Ala using ICM (Molsoft LLC, San Diego)<sup>61</sup>. Docking was performed by a Monte Carlo energy minimization procedure with a continuously flexible ligand and a grid representation of the ATP binding pocket that accounts for hydrophobic, electrostatic and hydrogen-bonding potentials. The top docking pose recapitulated the binding conformation of the shared scaffold co-crystallized with CDK2 (PDB: 4FKT). Ala 65 was then mutated back to wild type Lys and the preferred rotameric state of the Lys365 side-chain of ROP18 was identified by energy minimization in the internal coordinates space with ICM<sup>62</sup>. Separately, compound **7** was docked into the ROP18 crystal structure, using similar methods.

## Supplementary Material

Refer to Web version on PubMed Central for supplementary material.

## Acknowledgments

We are grateful to Drs. William Zuercher and David Drewry from GSK for providing access to the PKIS inhibitor sets and to Jennifer Barks for technical assistance. Supported in part by grants from the NIH (AI082423, AI118426). The SGC is a registered charity (number 1097737) that receives funds from AbbVie, Bayer Pharma AG, Boehringer Ingelheim, Canada Foundation for Innovation, Eshelman Institute for Innovation, Genome Canada, Innovative Medicines Initiative (EU/EFPIA) [ULTRA-DD grant no. 115766], Janssen, Merck & Co., Novartis Pharma AG, Ontario Ministry of Economic Development and Innovation, Pfizer, São Paulo Research Foundation-FAPESP, Takeda, and the Wellcome Trust.

## Abbreviations

|                                |   |
|--------------------------------|---|
| <b>ATF6<math>\beta</math></b>  | activating transcription factor 6 $\beta$ |
| <b>CDK1</b>                    | cyclin dependent kinase 2                 |
| <b>DMSO</b>                    | dimethyl sulfoxide                        |
| <b>HTS</b>                     | high throughput screening                 |
| <b>IFN-<math>\gamma</math></b> | interferon $\gamma$                       |
| <b>LD<sub>50</sub></b>         | lethal dose 50                            |
| <b>MCE</b>                     | microfluidic capillary electrophoresis    |
| <b>PKIS</b>                    | Published Kinase Inhibitor Set            |
| <b>PV</b>                      | parasitophorous vacuole                   |
| <b>PVM</b>                     | parasitophorous vacuole membrane          |
| <b>ROP</b>                     | rhopty protein                            |

## References

1. Dubey, JP. Toxoplasmosis of animals and humans. CRC Press; Boca Raton: 2010.
2. Jones JL, Dubey JP. Waterborne toxoplasmosis--recent developments. *Exp Parasitol.* 2010; 124:10–25. [PubMed: 19324041]

3. Jones JL, Dubey JP. Foodborne Toxoplasmosis. *Clin Infect Dis*. 2012; 55:864–851.
4. Montoya JG, Liesenfeld O. Toxoplasmosis. *Lancet*. 2004; 363:1965–1976. [PubMed: 15194258]
5. McCabe, RE. Antitoxoplasma chemotherapy. In: Joynson, DHM.; Wreghitt, TG., editors. *Toxoplasmosis: a comprehensive clinical guide*. Cambridge Univ. Press; Cambridge: 2001. p. 319-359.
6. Boyle JP, Rajasekar B, Saeij JPJ, Ajioka JW, Berriman M, Paulsen I, Sibley LD, White M, Boothroyd JC. Just one cross appears capable of dramatically altering the population biology of a eukaryotic pathogen like *Toxoplasma gondii*. *Proc Natl Acad Sci (USA)*. 2006; 103:10514–10519. [PubMed: 16801557]
7. Su C, Evans D, Cole RH, Kissinger JC, Ajioka JW, Sibley LD. Recent expansion of *Toxoplasma* through enhanced oral transmission. *Science*. 2003; 299:414–416. [PubMed: 12532022]
8. Khan A, Fux B, Su C, Dubey JP, Darde ML, Ajioka JW, Rosenthal BM, Sibley LD. Recent transcontinental sweep of *Toxoplasma gondii* driven by a single monomorphic chromosome. *Proc Natl Acad Sci (USA)*. 2007; 104:14872–14877. [PubMed: 17804804]
9. Lehmann T, Marcet PL, Graham DH, Dahl ER, Dubey JP. Globalization and the population structure of *Toxoplasma gondii*. *Proc Natl Acad Sci (USA)*. 2006; 103:11423–11428. [PubMed: 16849431]
10. Su CL, Khan A, Zhou P, Majumdar D, Ajzenberg D, Darde ML, Zhu XQ, Ajioka JW, Rosenthal B, Dubey JP, Sibley LD. Globally diverse *Toxoplasma gondii* isolates comprise six major clades originating from a small number of distinct ancestral lineages. *Proc Natl Acad Sci (USA)*. 2012; 109:5844–5849. [PubMed: 22431627]
11. Sibley LD, Qiu W, Fentress S, Taylor SJ, Khan A, Hui R. Forward genetics in *Toxoplasma gondii* reveals a family of rhoptyry kinases that mediates pathogenesis. *Eukaryot Cell*. 2009; 8:1085–1093. [PubMed: 19465561]
12. Saeij JPJ, Boyle JP, Collier S, Taylor S, Sibley LD, Brooke-Powell ET, Ajioka JW, Boothroyd JC. Polymorphic secreted kinases are key virulence factors in toxoplasmosis. *Science*. 2006; 314:1780–1783. [PubMed: 17170306]
13. Taylor S, Barragan A, Su C, Fux B, Fentress SJ, Tang K, Beatty WL, Haij EL, Jerome M, Behnke MS, White M, Wootton JC, Sibley LD. A secreted serine-threonine kinase determines virulence in the eukaryotic pathogen *Toxoplasma gondii*. *Science*. 2006; 314:1776–1780. [PubMed: 17170305]
14. Fentress SJ, Behnke MS, Dunay IR, Moashayekhi M, Rommereim LM, Fox BA, Bzik DJ, Taylor GA, Turk BE, Lichti CF, Townsend RR, Qiu W, Hui R, Beatty WL, Sibley LD. Phosphorylation of immunity-related GTPases by a parasite secretory kinase promotes macrophage survival and virulence. *Cell Host Microbe*. 2010; 16:484–495. [PubMed: 21147463]
15. Shen B, Brown KM, Lee TD, Sibley LD. Efficient gene disruption in diverse strains of *Toxoplasma gondii* using CRISPR/CAS9. *mBio*. 2014; 5(3):e011114–14. [PubMed: 24825012]
16. Khan A, Taylor S, Ajioka JW, Rosenthal BM, Sibley LD. Selection at a single locus leads to widespread expansion of *Toxoplasma gondii* lineages that are virulent in mice. *PLoS Genetics*. 2009; 5:e1000404. [PubMed: 19266027]
17. Behnke M, Khan A, Lauron EJ, Jimah J, Wang RQ, Tolia NH, Sibley LD. Rhoptyry proteins ROP5 and ROP18 are major murine virulence factors in genetically divergent South American strains of *Toxoplasma gondii*. *PLoS Genet*. 2015 in press.
18. Behnke MS, Khan A, Wootton JC, Dubey JP, Tang K, Sibley LD. Virulence differences in *Toxoplasma* mediated by amplification of a family of polymorphic pseudokinases. *Proc Natl Acad Sci (USA)*. 2011; 108:9631–9636. [PubMed: 21586633]
19. Reese ML, Zeiner GM, Saeij JP, Boothroyd JC, Boyle JP. Polymorphic family of injected pseudokinases is paramount in *Toxoplasma* virulence. *Proc Natl Acad Sci U S A*. 2011; 108:9625–9630. [PubMed: 21436047]
20. Hunter CA, Sibley LD. Modulation of innate immunity by *Toxoplasma gondii* virulence effectors. *Nat Rev Microbiol*. 2012; 10:766–778. [PubMed: 23070557]
21. Etheridge RD, Alagan A, Tang K, Turk BE, Sibley LD. ROP18 and ROP17 kinase complexes synergize to control acute virulence of *Toxoplasma* in the mouse. *Cell Host Microbe*. 2014; 15:537–550. [PubMed: 24832449]
22. Steinfeldt T, Konen-Waisman S, Tong L, Pawlowski N, Lamkemeyer T, Sibley LD, Hunn JP, Howard JC. Phosphorylation of mouse immunity-related GTPase (IRG) resistance proteins is an



- evasion strategy for virulent *Toxoplasma gondii*. PLoS Biol. 2010; 8:e1000576. [PubMed: 21203588]
23. Khaminets A, Hunn JP, Konen-Waisman S, Zhao YO, Preukschat D, Coers J, Boyle JP, Ong YC, Boothroyd JC, Reichmann G, Howard JC. Coordinated loading of IRG resistance GTPases on to the *Toxoplasma gondii* parasitophorous vacuole. Cell Microbiol. 2010; 12:939–961. [PubMed: 20109161]
  24. Zhao Y, Ferguson DJ, Wilson DC, Howard JC, Sibley LD, Yap GS. Virulent *Toxoplasma gondii* evade immunity-related GTPase-mediated parasite vacuole disruption within primed macrophages. J Immunol. 2009; 182:3775–3781. [PubMed: 19265156]
  25. Zhao YO, Khaminets A, Hunn JP, Howard JC. Disruption of the *Toxoplasma gondii* parasitophorous vacuole by IFN-gamma-inducible immunity-related GTPases (IRG proteins) triggers necrotic cell death. PLoS Pathog. 2009; 5:e1000288. [PubMed: 19197351]
  26. Behnke MS, Fentress SJ, Mashayekhi M, Li LL, Taylor GA, LDS. The polymorphic pseudokinase ROP5 controls virulence in *Toxoplasma gondii* by regulating the active kinase ROP18. PLoS Path. 2012; 8:e1002992.
  27. Fleckenstein MC, Reese ML, Konen-Waisman S, Boothroyd JC, Howard JC, Steinfeldt T. A *Toxoplasma gondii* Pseudokinase Inhibits Host IRG Resistance Proteins. PLoS Biol. 2012; 10:e1001358. [PubMed: 22802726]
  28. Niedelman W, Gold DA, Rosowski EE, Sprockholt JK, Lim D, Farid Arenas A, Melo MB, Spooner E, Yaffe MB, Saeij JP. The rhopty proteins ROP18 and ROP5 mediate *Toxoplasma gondii* evasion of the murine, but not the human, interferon-gamma response. PLoS Path. 2012; 8:e1002784.
  29. Yamamoto M, Ma JS, Mueller C, Kamiyama N, Saiga H, Kubo E, Kimura T, Okamoto T, Okuyama M, Kayama H, Nagamune K, Takashima S, Matsuura Y, Soldati-Favre D, Takeda K. ATF6-beta is a host cellular target of the *Toxoplasma gondii* virulence factor ROP18. J Exp Med. 2011; 208:1533–1546. [PubMed: 21670204]
  30. Howard JC, Hunn JP, Steinfeldt T. The IRG protein-based resistance mechanism in mice and its relation to virulence in *Toxoplasma gondii*. Curr Opin Microbiol. 2011; 14:414–421. [PubMed: 21783405]
  31. Sanchez V, de-la-Torre A, Gomez-Marin JE. Characterization of ROP18 alleles in human toxoplasmosis. Parasitology international. 2014; 63:463–469. [PubMed: 24177250]
  32. Miranda-Saavedra D, Gabaldon T, Barton GJ, Langsley G, Doerig C. The kinomes of apicomplexan parasites. Microbes Infect. 2012; 14:796–810. [PubMed: 22587893]
  33. Wu P, Nielsen TE, Clausen MH. FDA-approved small-molecule kinase inhibitors. Trends in pharmacological sciences. 2015; 36:422–439. [PubMed: 25975227]
  34. Lucet IS, Tobin A, Drewry D, Wilks AF, Doerig C. Plasmodium kinases as targets for new-generation antimalarials. Future Med Chem. 2012; 4:2295–2310. [PubMed: 23234552]
  35. Tewari R, Straschil U, Bateman A, Bohme U, Cherevach I, Gong P, Pain A, Billker O. The systematic functional analysis of Plasmodium protein kinases identifies essential regulators of mosquito transmission. Cell Host Microbe. 2010; 8:377–387. [PubMed: 20951971]
  36. Solyakov L, Halbert J, Alam MM, Semblat JP, Dorin-Semblat D, Reiningger L, Bottrill AR, Mistry S, Abdi A, Fennell C, Holland Z, Demarta C, Bouza Y, Sicard A, Nivez MP, Eschenlauer S, Lama T, Thomas DC, Sharma P, Agarwal S, Kern S, Pradel G, Graciotti M, Tobin AB, Doerig C. Global kinomic and phospho-proteomic analyses of the human malaria parasite Plasmodium falciparum. Nat Commun. 2011; 2:565. [PubMed: 22127061]
  37. Bradley PJ, Ward C, Cheng SJ, Alexander DL, Collier S, Coombs GH, Dunn JD, Ferguson DJ, Sanderson SJ, Wastling JM, Boothroyd JC. Proteomic analysis of rhopty organelles reveals many novel constituents for host-parasite interactions in *T. gondii*. J Biol Chem. 2005; 280:34245–34258. [PubMed: 16002398]
  38. Peixoto L, Chen F, Harb OS, Davis PH, Beiting DP, Brownback CS, Ouluguem D, Roos DS. Integrative genomics approaches highlight a family of parasite-specific kinases that regulate host responses. Cell Host Microbe. 2010; 8:208–218. [PubMed: 20709297]
  39. Talevich E, Kannan N. Structural and evolutionary adaptation of rhopty kinases and pseudokinases, a family of coccidian virulence factors. BMC Evol Biol. 2013; 13:117. [PubMed: 23742205]

40. Qiu W, Wernimont A, Tang K, Taylor S, Lunin V, Schapira M, Fentress SJ, Hui R, Sibley LD. Novel structural and regulatory features of rhoptyry secretory kinases in *Toxoplasma gondii*. *EMBO J*. 2008; 28:969–979. [PubMed: 19197235]
41. Reese ML, Boothroyd JC. A conserved non-canonical motif in the pseudoactive site of the ROP5 pseudokinase domain mediates its effect on *Toxoplasma* virulence. *J Biol Chem*. 2011; 286:29366–29375. [PubMed: 21708941]
42. Clatworthy AE, Pierson E, Hung DT. Targeting virulence: a new paradigm for antimicrobial therapy. *Nat Chem Biol*. 2007; 3:541–548. [PubMed: 17710100]
43. Bernasconi P, Min Chen Galasinski S, Popa-Burke I, Bobasheva A, Coudurier L, Birkos S, Hallam R, Janzen WP. A Chemogenomic Analysis of the Human Proteome: Application to Enzyme Families. *Journal of Biomolecular Screening*. 2007; 12:972–982. [PubMed: 17942790]
44. Pommereau A, Pap E, Kannt A. Two Simple and Generic Antibody-Independent Kinase Assays: Comparison of a Bioluminescent and a Microfluidic Assay Format. *Journal of Biomolecular Screening*. 2004; 9:409–416. [PubMed: 15296640]
45. Blackwell LJ, Birkos S, Hallam R, Van De Carr G, Arroway J, Suto CM, Janzen WP. High-throughput screening of the cyclic AMP-dependent protein kinase (PKA) using the caliper microfluidic platform. *Methods Mol Biol*. 2009; 565:225–237. [PubMed: 19551365]
46. Kotturi P, Boudreau M. Mobility shift screening assays for protein kinase targets. *American Laboratory*. 2003; 35:32–+.
47. Sundberg SA, Chow A, Nikiforov T, Wada HG. Microchip-based systems for target validation and HTS. *Drug Discov Today*. 2000; 5:92–103. [PubMed: 11564572]
48. Zhang J-H, Chung TD, Oldenburg KR. A simple statistical parameter for use in evaluation and validation of high throughput screening assays. *Journal of biomolecular screening*. 1999; 4:67–73. [PubMed: 10838414]
49. Hutti JE, Porter MA, Cheely AW, Cantley LC, Wang X, Kireev D, Baldwin AS, Janzen WP. Development of a high-throughput assay for identifying inhibitors of TBK1 and IKKepsilon. *PLoS one*. 2012; 7:e41494. [PubMed: 22859992]
50. Peterson EJ, Janzen WP, Kireev D, Singleton SF. High-Throughput Screening for RecA Inhibitors Using a Transcreeper Adenosine 5'-O-Diphosphate Assay. *Assay and drug development technologies*. 2012; 10:260–268. [PubMed: 22192312]
51. Drewry DH, Willson TM, Zuercher WJ. Seeding collaborations to advance kinase science with the GSK Published Kinase Inhibitor Set (PKIS). *Current topics in medicinal chemistry*. 2014; 14:340. [PubMed: 24283969]
52. Lim D, Gold DA, Julien L, Rosowski EE, Niedelman W, Yaffe MB, Saeij JP. Structure of the *Toxoplasma gondii* ROP18 kinase domain reveals a second ligand binding pocket required for acute virulence. *J Biol Chem*. 2013; 288:34968–34980. [PubMed: 24129568]
53. Bramson HN, Corona J, Davis ST, Dickerson SH, Edelstein M, Frye SV, Gampe RT Jr, Harris PA, Hassell A, Holmes WD, Hunter RN, Lackey KE, Lovejoy B, Luzzio MJ, Montana V, Rocque WJ, Rusnak D, Shewchuk L, Veal JM, Walker DH, Kuyper LF. Oxindole-based inhibitors of cyclin-dependent kinase 2 (CDK2): design, synthesis, enzymatic activities, and X-ray crystallographic analysis. *Journal of medicinal chemistry*. 2001; 44:4339–4358. [PubMed: 11728181]
54. Drewry DH, Willson TM, Zuercher WJ. Seeding collaborations to advance kinase science with the GSK Published Kinase Inhibitor Set (PKIS). *Curr Top Med Chem*. 2014; 14:340–342. [PubMed: 24283969]
55. Gamo FJ, Sanz LM, Vidal J, de Cozar C, Alvarez E, Lavandera JL, Vanderwall DE, Green DV, Kumar V, Hasan S, Brown JR, Peishoff CE, Cardon LR, Garcia-Bustos JF. Thousands of chemical starting points for antimalarial lead identification. *Nature*. 2010; 465:305–310. [PubMed: 20485427]
56. Feng BY, Shelat A, Doman TN, Guy RK, Shoichet BK. High-throughput assays for promiscuous inhibitors. *Nature chemical biology*. 2005; 1:146–148. [PubMed: 16408018]
57. Keenan SM, Geyer JA, Welsh WJ, Prigge ST, Waters NC. Rational inhibitor design and iterative screening in the identification of selective plasmodial cyclin dependent kinase inhibitors. *Combinatorial chemistry & high throughput screening*. 2005; 8:27–38. [PubMed: 15720195]

58. Behnke MS, Khan A, Sibley LD. Genetic mapping reveals that sinefungin resistance in *Toxoplasma gondii* is controlled by a putative amino acid transporter locus that can be used as a negative selectable marker. *Eukaryot Cell*. 2014
59. Papic N, Hunn JP, Pawlowski N, Zerrahn J, Howard JC. Inactive and active states of the interferon-inducible resistance GTPase, Irga6, in vivo. *J Biol Chem*. 2008; 283:32143–32151. [PubMed: 18784077]
60. Starnes GL, Jewett TJ, Carruthers VB, Sibley LD. Two separate, conserved acidic amino acid domains within the *Toxoplasma gondii* MIC2 cytoplasmic tail are required for parasite survival. *J Biol Chem*. 2006; 281:30745–30754. [PubMed: 16923803]
61. Neves MA, Totrov M, Abagyan R. Docking and scoring with ICM: the benchmarking results and strategies for improvement. *Journal of computer-aided molecular design*. 2012; 26:675–686. [PubMed: 22569591]
62. Abagyan R, Totrov M. Biased probability Monte Carlo conformational searches and electrostatic calculations for peptides and proteins. *J Mol Biol*. 1994; 235:983–1002. [PubMed: 8289329]

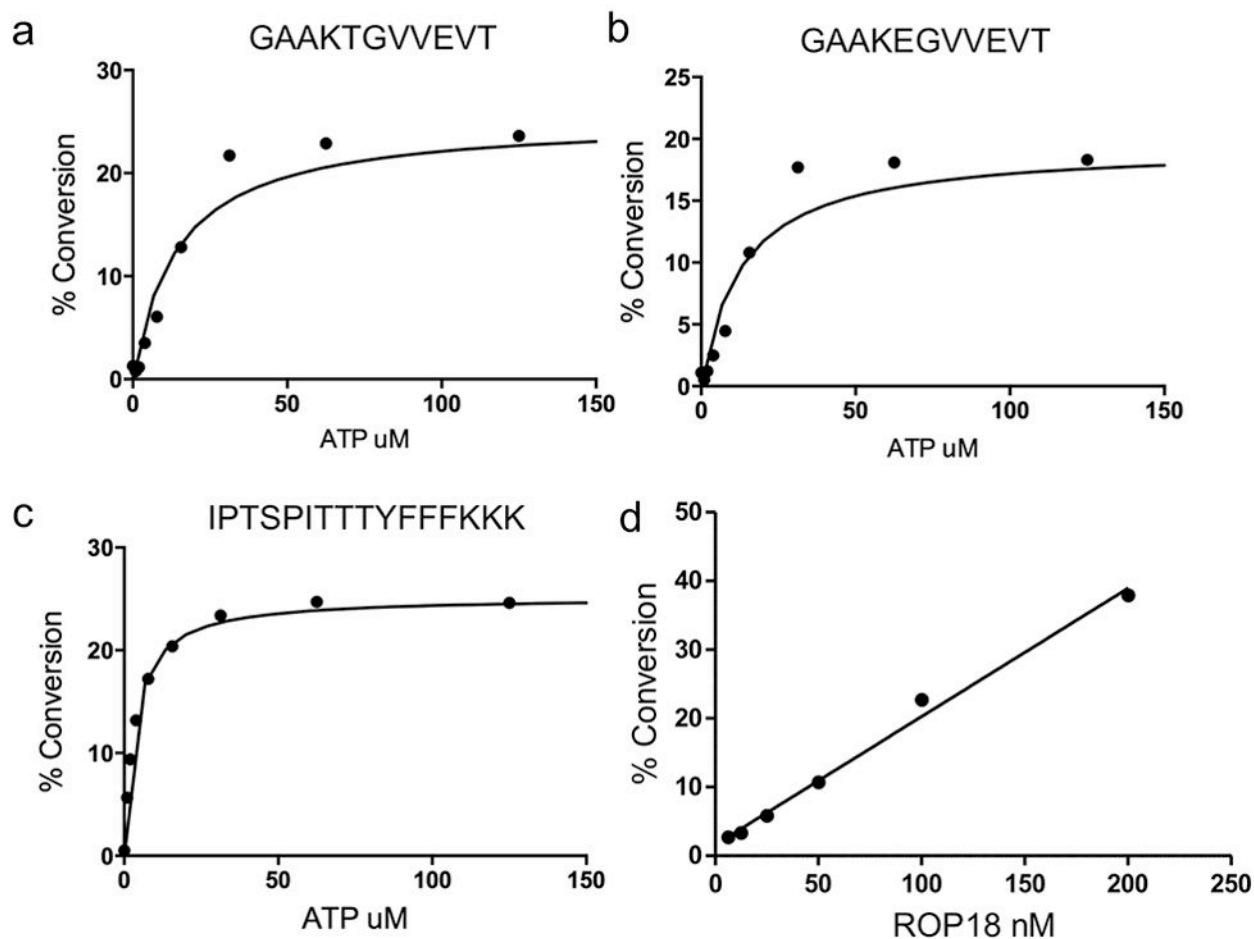


**Figure 1.**

Kinetic analysis of ROP18 kinase. Determination of the apparent ATP  $K_m$  for three fluorescently labeled ROP18 substrates in their respective microfluidic assays: (a) FL-T, a native ROP18 substrate peptide from Irga6 (b) FL-E, a threonine point mutation of the native peptide from Irga6, and (c) FL-8, an unrelated peptide substrate. Percent substrate conversion to phosphorylated product was plotted against ATP concentration and fit to the Michaelis-Menton equation to determine the ATP apparent  $K_m$  for each of the three substrates. All titrations contained 1  $\mu$ M peptide; a and b were conducted with 50 nM ROP18, while c was conducted with ~15 nM ROP18. (d) Determination of optimal enzyme concentration for assay. Recombinant ROP18 kinase was titrated using FL-T substrate to determine the amount of enzyme needed to obtain ~30% conversion to phosphorylated product after a 3 h room temperature incubation.

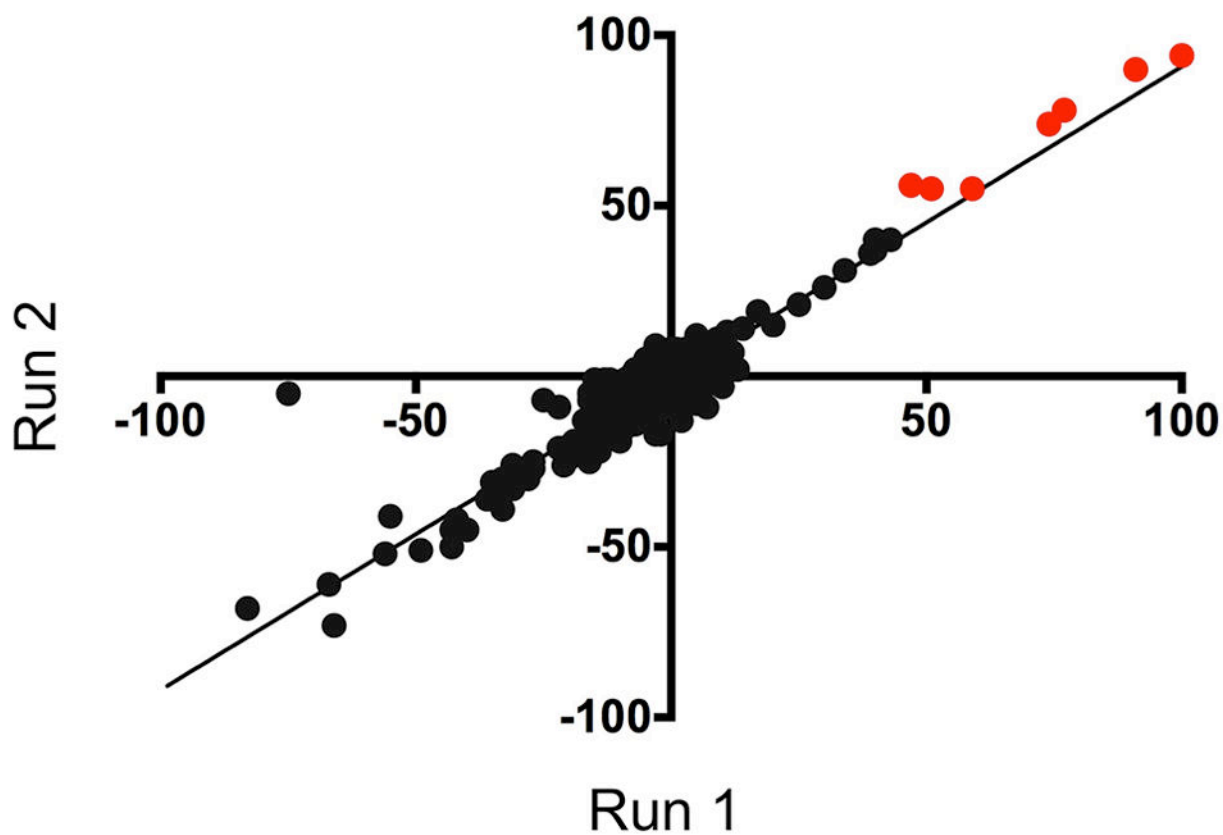


**Figure 2.** Reproducibility of the Caliper assay for ROP18. Duplicate runs of the PKIS (Public Kinase Inhibitor Set, GSK) were plotted on separate axes to assess the reproducibility of the assay. Compounds with inhibitory activity are marked in red. Linear regression,  $r^2 = 0.87$ .

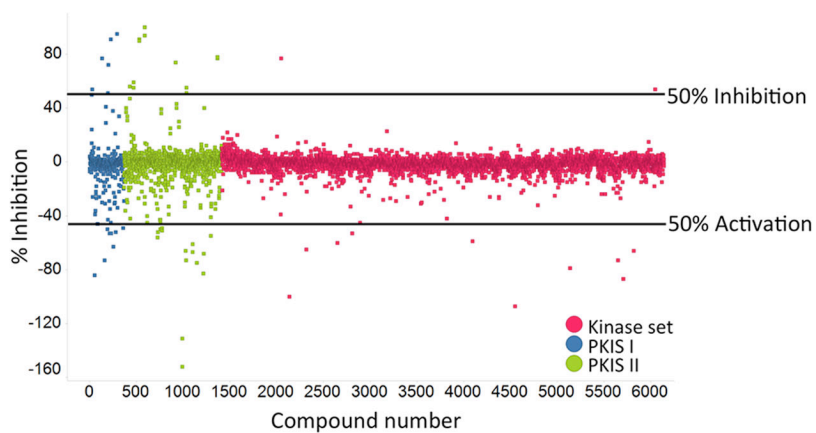


**Figure 3.** Summary of high-throughput screening data. Percent inhibition of ROP18 phosphorylation of FL-T was plotted for the three compound libraries screened. Compounds with inhibition 50% activity threshold (black line) were reconfirmed and tested for  $IC_{50}$  concentrations (Table 1). Compounds where the enzymatic activity of ROP18 increased by more than 50% above the baseline control were considered activators (black line)

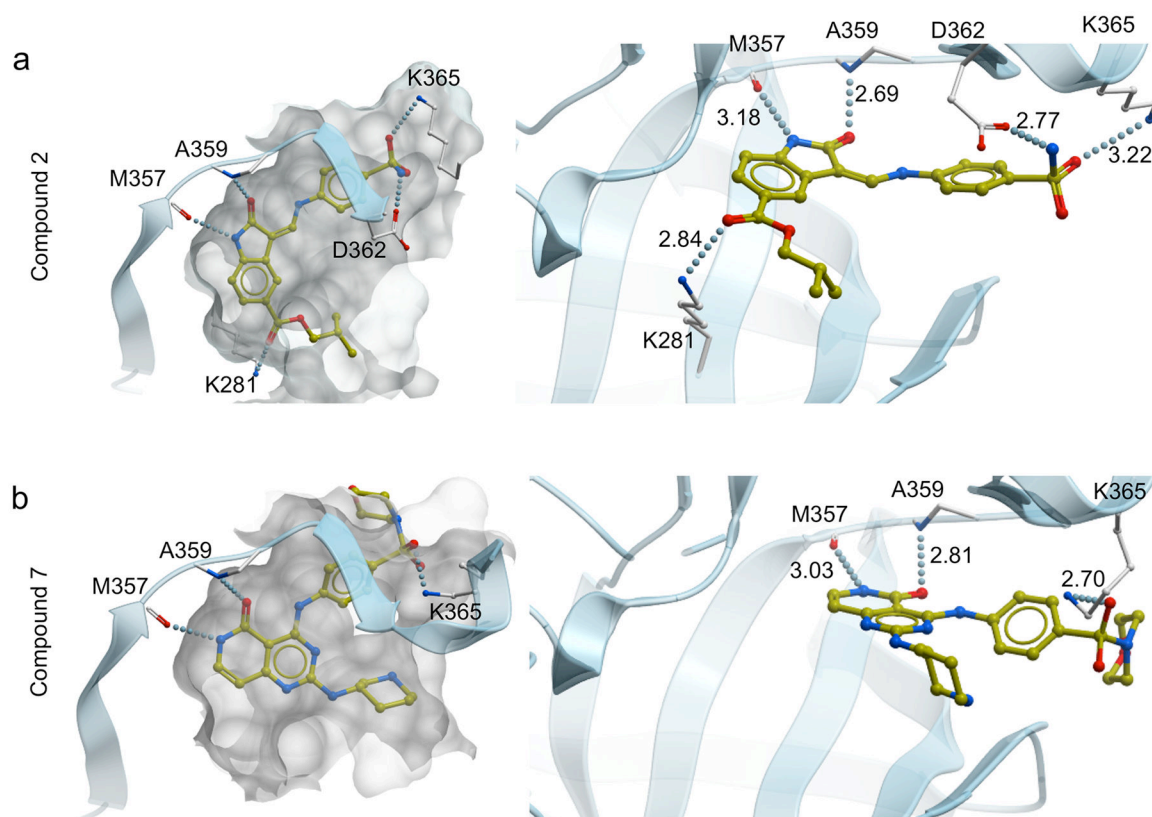


**Figure 4.** Docking model of compounds **2** and **7** bound to ROP18 (PDB: 4JRN). (a) Compound **2** (mustard) occupies the ATP binding pocket of ROP18 (light blue), making extensive hydrogen bonds with surrounding side-chains and the backbone of the hinge region (M357, A359). Additionally the sulfonamide group makes hydrogen bonds with D362 and K365 from the C-lobe. (b) Similarly, compound **7** binds to M357 and A 359 in the hinge region and interacts with K365 in the C-lobe.

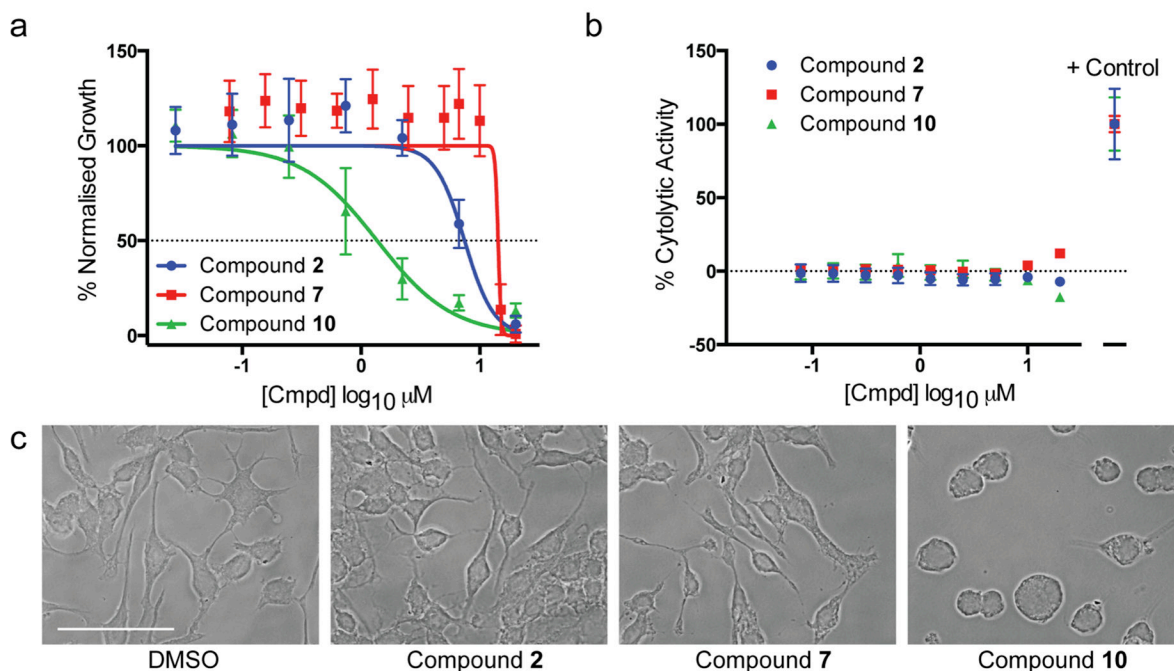


**Figure 5.** Cellular toxicity screening. (a) Inhibition of cell proliferation using an MTS-based assay developed 48 h after compound addition to RAW264.7 macrophages. Data points indicate mean  $\pm$  SD, N=3 experiments, n=9 total data points. (b) LDH-release assay to detect acute cytolytic activity of compounds on RAW264.7 macrophages after 4 h exposure. Data points indicate mean  $\pm$  SD, N=3 experiments, n=9 total data points. (c) Phase contrast microscopy depicting morphological disruption caused by 10  $\mu$ M compound **10** after 30 min incubation, scale-bar denotes 50 microns.



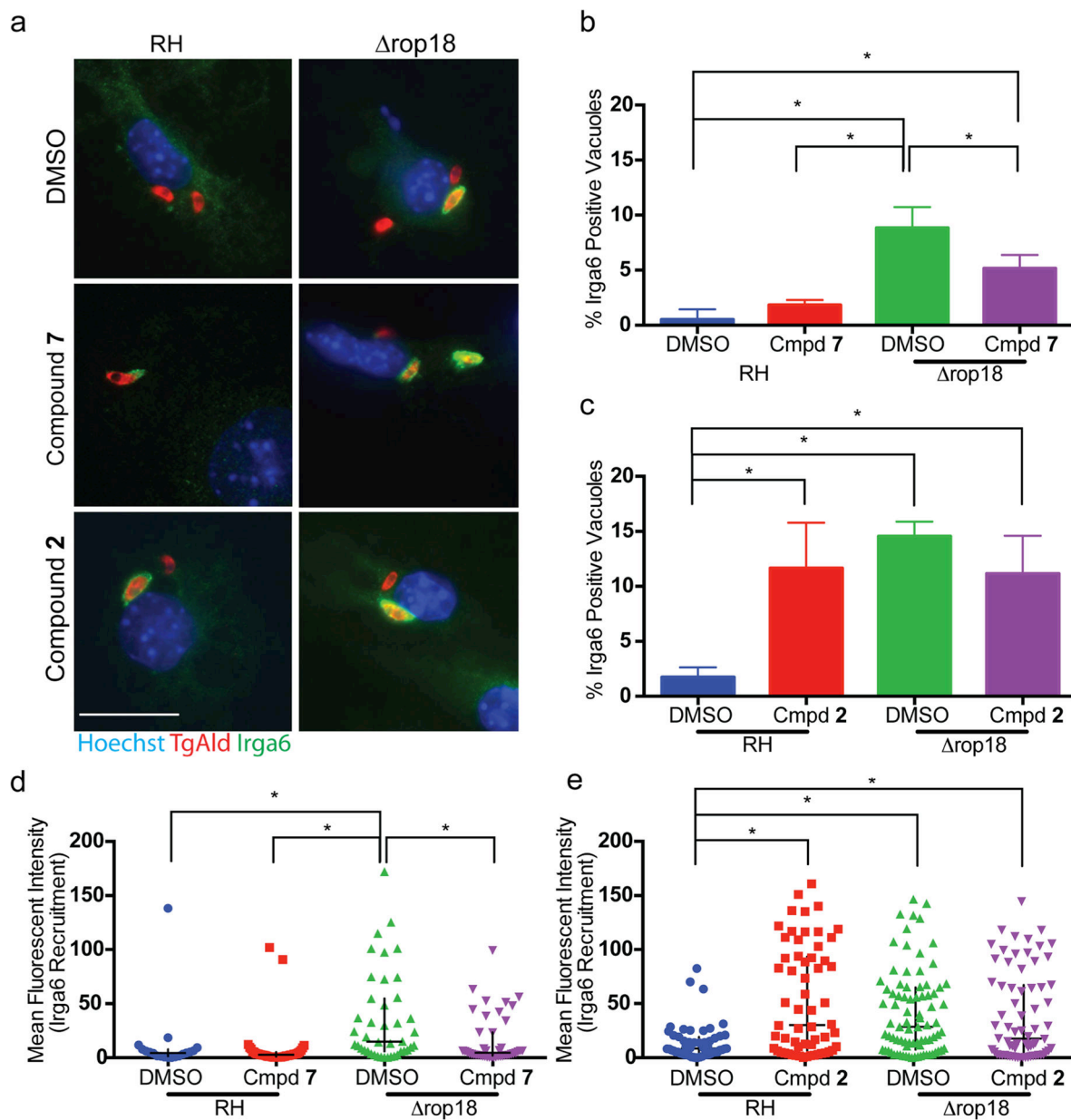


**Figure 6.** Biological validation of ROP18 inhibitors. (a) Qualitative immuno-fluorescence microscopy demonstrating the recruitment of Irga6 to parasitophorous vacuoles (PV) in activated (100 U/ml IFN $\gamma$  / 1 ng/ml LPS) RAW macrophages. Parasites were detected by labeling with rabbit anti-TgAldolase (secondary antibody: Alexi Fluor 594) loading of Irga6 was detected using the mouse maybe 10D7 (secondary antibody: Alexi Fluor488). Nuclei were labeled with Hoechst 33258, scale-bar denotes 20  $\mu$ m. (b, c) Visual scoring of Irga6 positive vacuoles surrounding wild type (RH) or *rop18* parasites in the presence of compound 7, compound 2, or 0.1% DMSO vehicle control. Bars indicate mean  $\pm$  standard deviation, data were analyzed by ANOVA with Holm-Side multiple comparison correction. Significant differences ( $P$  0.05) are denoted by \*; for clarity non-significant comparisons are not

indicated. (d) Quantification of Irga6 loading to the PV of wild type (RH) or *rop18* parasites in the presence of compound **7** or 0.1% DMSO vehicle control. Background fluorescence was subtracted and parasites with negative values were removed from the analysis, data were analyzed using a Kruskal-Wallis non-parametric test, multiple comparisons were conducted using Dunn's correction,  $P < 0.05$ . Bars indicate median  $\pm$  interquartile range, significant differences ( $P < 0.05$ ) are denoted by \*. (e) Quantification of Irga6 loading to the PV of wild type (RH) or *rop18* parasites in the presence of compound **2** or 0.1% DMSO vehicle control, data analysis as previously described for compound **7**.

Author Manuscript

Author Manuscript

Author Manuscript

Author Manuscript

**Table 1**

Assay Conditions for microfluidic mobility shift ROP18 assay.

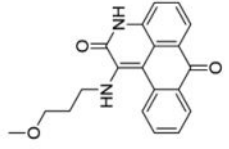
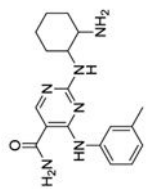
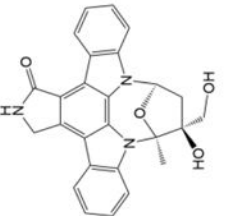
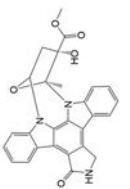
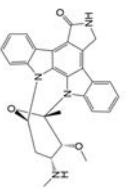
|                       |   |
|-----------------------|---|
| Assay buffer          | 50 mM HEPES pH 7.4, 0.01% Triton X-100, 10mM MgCl <sub>2</sub>  |
| Separation buffer     | ProfilerPro separation buffer with 0.5% coating reagent 8 (CR-8)  |
| Separation conditions | -100 V downstream voltage, -1000 V upstream voltage, -1.0 psi pressure, post-sample sip time of 29 seconds, and final delay of 110 seconds.                                       |
| Enzyme                | 75 nM, prepared in assay buffer 1 mM DTT  |
| Substrate             | 1 μM prepared in assay buffer with 60 μM ATP (4x K <sub>m</sub> )   |
| Endpoint assay setup  | 4.5 μL 2.2x enzyme solution added to compound plate (1 μL of 1 mM in 10% DMSO), incubate 10 minutes, 4.5 μL 2.2x substrate solution added, incubate 3 h, 20μL stop solution added |
| Incubation            | 3 h at room temperature   |
| Reaction plate        | Nunc shallow 384 well   |
| Stop solution         | 70 mM EDTA, pH 7.5 in assay buffer  |

Table 2

Summary of confirmed ROP18 inhibitors tested with three substrates.

| Compound # | Chemical name  | Compound IDs                | Scaffold | R1 | R2 | IC50 $\mu$ Md |      |      |
|------------|--|-----------------------------|----------|----|----|---------------|------|------|
|            |  |                             |          |    |    | EL-T          | EL-E | EL-R |
| 1          | 4-[(7-hydroxy-6H-pyrido[2,3-g][1,3]benzothiazol-8-yl)methyl]neamino]benzenesulfonamide                   | UNC1012685A<br>GW297361X    |          |    |    | 2.93          | 2.48 | 1.21 |
| 2          | isobutyl 2-hydroxy-3-[(4-sulfamoylphenyl)iminomethyl]-1H-indole-5-carboxylate                            | UNC1012749A<br>GW416981X    |          |    |    | 0.17          | 0.29 | 0.51 |
| 3          | 2-hydroxy-N-(3-hydroxy-2,2-dimethyl-propyl)-3-(4-sulfamoylphenyl)azo-1H-indole-5-carboxamide             | UNC1012606A<br>GW301784X    |          |    |    | 0.39          | 0.19 | 0.65 |
| 4          | 2-hydroxy-N-(4-pyridylmethyl)-3-(4-sulfamoylphenyl)azo-1H-indole-5-carboxamide                           | UNC1012753A<br>GW30657X     |          |    |    | 8.13          | 2.66 | >10  |
| 5          | 4-[(1,1-dioxo-2,3-dihydrobenzothiazophen-6-yl)amino]-2-(pyrrolidin-3-ylamino)pyrido[4,3-d]pyrimidin-5-ol | UNC10225451A<br>GSK2181386A |          |    |    | >10           | 4.02 | >10  |
| 6          | 4-(3,5-dichlorophenyl)-2-(pyrrolidin-3-ylamino)pyrido[4,3-d]pyrimidin-5-ol                               | UNC1022257A<br>GSK2188764A  |          |    |    | >10           | 7.49 | >10  |

| Compound # | Chemical name  | Compound IDs                              | Scaffold | R1 | R2 | IC50 $\mu$ M <sup>d</sup> |      |      |
|------------|--|---|----------|----|----|---------------------------|------|------|
|            |  |   |          |    |    | FL-T                      | FL-E | FL-S |
| 7          | 4-(4-morpholinylsulfonyl)amino)-2-(3-peroxybutyl)pyridine(4,3-c)pyrimidin-5-ol   | UNC10225269A<br>GSK217277A <sup>b</sup>   |          |    |    | 0.30                      | 0.18 | 0.40 |
| 8          | 2,6-difluoro-4-N-(1-(3-(3-(2-sulfamoyl)butyl)amino)pyrimidin-4-yl)pyrazolo[1,5-a]pyridin-2-yl)phenyl)benzamide           | UNC10224988A<br>GSK336735A <sup>b</sup>   |          |    |    | 0.69                      | 0.94 | 0.63 |
| 9          | 4-N-(1-(3-(3-(2-(4-(methylsulfonyl)methyl)amino)pyrimidin-4-yl)pyrazolo[1,5-b]pyridazin-2-yl)phenyl)isobutanecarboxamide | UNC10223159A<br>GSK330559A <sup>b</sup>   |          |    |    | 6.98                      | >10  | >10  |
| 10         | 2,6-difluoro-4-N-(1-(3-(3-(2-(4-(methylsulfonylmethyl)amino)pyrimidin-4-yl)pyrazolo[1,5-a]pyridin-2-yl)phenyl)benzamide  | UNC10225246A<br>GSK3323543A <sup>b</sup>  |          |    |    | 0.44                      | 1.00 | 2.83 |
| 11         | 1-(3-(3,3-dimethyl-2-oxo-butyl)sulfanyl)-1,2,4-thiadiazol-5-yl)-3-(4-methoxyphenyl)urea                                  | UNC10101795A<br>AST 07114923 <sup>c</sup> |          |    |    | >10                       | 6.44 | >10  |

| Compound # | Chemical name   | Compound IDs                                   | Scaffold   | R1 | R2 | IC50 $\mu$ M <sup>d</sup> |      |      |
|------------|---|--|--|----|----|---------------------------|------|------|
|            |   |  |  |    |    | FL-T                      | FL-E | FL-S |
| 12         | 17-(3-methoxyethylamino)-20-azetetracycloheptadec-1,3(6),4(11),5(12),7(14),13(15),16-heptaene-18,19-dione   | UNC10104516A<br>FI14141229 <sup>d</sup>        |    | -  | -  | >10                       | >10  | >10  |
| 13         | 2-((2-aminocyclohexyl)amino)-4-(5-methylamino)pyrimidine-5-carboxamide  | UNC1022280A<br>GSK98610C <sup>b</sup>          |    | -  | -  | 2.98                      | 6.66 | >10  |
| 14         | Lesaurinib (5S,6S,8R)-6-hydroxy-6-(hydroxymethyl)-5-methyl-5,6,7,8,14,15-hexahydro-13H-16-oxa-4b,8a,14-triazas-5,8-methanodibenzo[ <i>b</i> , <i>h</i> ]cycloocta[ <i>jk</i> ]1-cyclopenta[ <i>l</i> ]as-indacene-13-one        | UNC10126572<br>Known Kinase Inhibitor<br>Plate |    | -  | -  | 0.16                      | ND   | ND   |
| 15         | K252a Methyl (5S,6S,8R)-6-hydroxy-5-methyl-1,3-oxa-5,6,7,8,14,15-hexahydro-13H-16-oxa-4b,8a,14-triazas-5,8-methanodibenzo[ <i>b</i> , <i>h</i> ]cycloocta[ <i>jk</i> ]1-cyclopenta[ <i>l</i> ]as-indacene-6-carboxylate         | UNC10126570<br>Known Kinase Inhibitor<br>Plate |   | -  | -  | 0.059                     | ND   | ND   |
| 16         | Staurosporine (5S,6R,7R,9R)-6-methoxy-5-methyl-7-(methylamino)-6,7,8,9,15,16-hexahydro-5H,14H,17-oxa-4b,9a,15-triazas-5,9-methanodibenzo[ <i>b</i> , <i>h</i> ]cycloocta[ <i>jk</i> ]1-cyclopenta[ <i>l</i> ]as-indacene-14-one | UNC10126581<br>Known Kinase Inhibitor<br>Plate |  | -  | -  | 1.2                       | ND   | ND   |

<sup>a</sup> GSK Public Kinase Inhibitor Set I,<sup>b</sup> GSK Public Kinase Inhibitor Set II,

<sup>d</sup>FL-T, FL-E, and FL-8 refer to three different peptide substrates as defined in the methods.

<sup>e</sup>Asinex,  
<sup>f</sup>Life Chemicals, ND, Not done,

Author Manuscript

Author Manuscript

Author Manuscript

Author Manuscript